NANO LETTERS

Letter

pubs.acs.org/NanoLett

Growth of Close-Packed Semiconducting Single-Walled Carbon Nanotube Arrays Using Oxygen-Deficient TiO_2 Nanoparticles as Catalysts

Lixing Kang,[†,‡] Yue Hu,[†] Lili Liu,[§,∥] Juanxia Wu,[†] Shuchen Zhang,[†] Qiuchen Zhao,[†] Feng Ding,[§,⊥] Qingwen Li,*[,‡] and Jin Zhang*[,†]

[†]Center for Nanochemistry, Beijing National Laboratory for Molecular Sciences, Key Laboratory for the Physics and Chemistry of Nanodevices, State Key Laboratory for Structural Chemistry of Unstable and Stable Species, College of Chemistry and Molecular Engineering, Peking University, Beijing 100871, P.R. China

[‡]Key Laboratory of Nanodevices and Applications, Suzhou Institute of Nanotech and Nanobionics, Chinese Academy of Science, Suzhou, 215123, P.R. China

[§]Beijing Computational Science Research Center, Beijing 100084, P.R. China

[∥]Department of Chemistry, School of Science, Beijing Technology and Business University, Beijing 100048, P.R. China

[⊥]Institute of Textiles and Clothing, Hong Kong Polytechnic University, Kowloon, Hong Kong, P.R. China

Supporting Information

ABSTRACT: For the application of single-walled carbon nanotubes (SWNTs) in nanoelectronic devices, techniques to obtain horizontally aligned semiconducting SWNTs (s-SWNTs) with higher densities are still in their infancy. We reported herein a rational approach for the preferential growth of densely packed and well-aligned s-SWNTs arrays using oxygen-deficient TiO_2 nanoparticles as catalysts. Using this approach, a suitable concentration of oxygen vacancies in TiO_2 nanoparticles could form by optimizing the flow rate of hydrogen and carbon sources during the process of SWNT growth, and then horizontally aligned SWNTs with the density of ~10 tubes/μm and the s-SWNT percentage above 95% were successfully obtained on ST-cut quartz substrates. Theoretical calculations indicated that TiO_2 nanoparticles with a certain concentration of oxygen vacancies have a lower formation energy between s-SWNT than metallic SWNT (m-SWNT), thus realizing the preferential growth of s-SWNT arrays. Furthermore, this method can also be extended to other semiconductor oxide nanoparticles (i.e., ZnO, ZrO_2 and Cr_2O_3) for the selective growth of s-SWNTs, showing clear potential to the future applications in nanoelectronics.

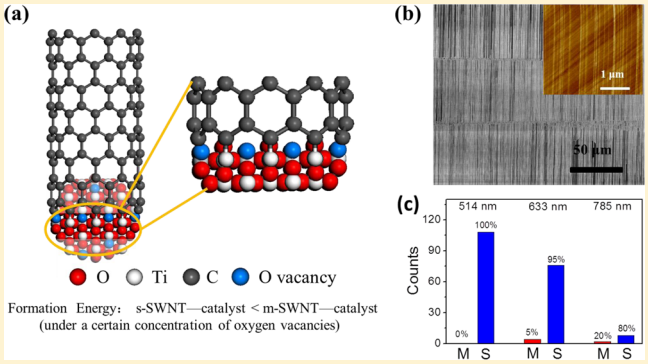

KEYWORDS: *Semiconducting single-walled carbon nanotube arrays, titanium dioxide catalysts, oxygen vacancy, preferential growth*

Close packed horizontally aligned single-walled carbon nanotube (SWNT) arrays with semiconducting properties are highly desirable for the fabrication of future electronic devices, especially for SWNTs-based integrated circuits (ICs).[1−3] In 2013, the researchers of IBM stated that, in order to realize SWNTs based ICs applications, the close-packed SWNT arrays should have ≥99.9999% s-SWNT purity with the density higher than 125 tubes/μm.[4] There are two kinds of approaches to solve these problems. One is the post-treatment method, in which nanotubes are first separated in solution and then assembled into aligned arrays.[5,6] These processes always introduce defects and contamination to the SWNTs which dramatically degrade the performance of devices. By contrast, direct growth approach by chemical vapor deposition (CVD) is a more promising strategy that provides high-quality SWNT arrays.[7,8] However, achieving a high purity of s-SWNT arrays with the required density by the direct growth method is still in its infancy.

During the past few decades, significant advances in the growth of horizontally aligned SWNTs have been witnessed.[9,10] The density of SWNT arrays has reached 10−50 tubes/μm by using single growth,[11] multiple-cycle growth,[12] multiple loading catalyst,[13] and periodic growth.[14] However, all of these methods can only produce mixtures of m-SWNTs and s-SWNTs, which largely decrease the performance of devices. To solve this problem, introducing water,[15] oxygen,[16] UV-light,[17,18] ceria supports,[19] or using ethanol/methanol[8] or isopropyl alcohol[7] as carbon sources during the CVD process to create a

Received: September 29, 2014
Revised: December 3, 2014
Published: December 24, 2014

DOI: 10.1021/nl5037325
Nano Lett. 2015, 15, 403−409

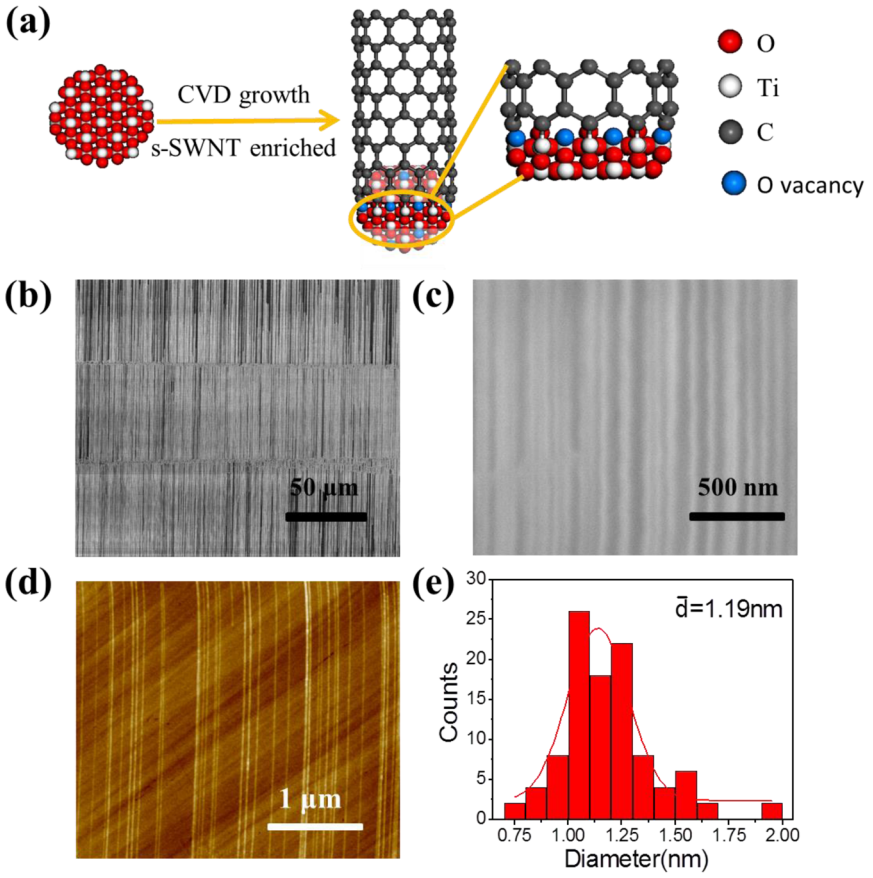

Figure 1. (a) Schematic illustration of selective growth of s-SWNTs by oxygen-deficient TiO_2 nanoparticles; (b–c) SEM images of the SWNT arrays using TiO_2 nanoparticles as catalysts under the growth condition of 200 sccm hydrogen and 200 sccm argon (through an ethanol bubbler); (d) typical AFM image of the as-grown SWNT arrays; (e) the corresponding diameter distribution of the SWNTs.

suitable oxidative environment for etching m-SWNTs were reported. Accordingly, SWNT arrays with 90–97% s-SWNT purity were obtained. However, these etching strategies severely limit the density of attained s-SWNT arrays; typical results are often below 5 tubes/um. Therefore, a direct selective growth of s-SWNT arrays with higher density remains a big challenge.

Besides the above growth process, the catalyst is another extremely important factor affecting SWNTs nucleation and growth.[20] Many metals and their alloys, such as Co,[21] FeCu,[22] and WCo,[23] have been verified to favor the growth of random semiconducting SWNTs. However, metal catalyst particles are usually in a liquid or partial liquid state with fluctuating sizes and structures, which make it difficult to obtain SWNT arrays with a predefined and precisely controlled structure. Meanwhile, the residual metallic catalysts severely limit the applications of SWNTs in many fields. Recently, many nonmetallic nanoparticles have been investigated as the catalysts for SWNT growth.[24−26] TiO_2, a well-known nanomaterial, shows excellent catalytic performance in many fields.[27−29] According to the Ellingham diagram for oxides, TiO_2 is extremely stable and not expected to be reduced in SWNT growth conditions.[30] Nevertheless, due to the nanometer size effect, some oxygen vacancies formed in TiO_2, and their concentrations can be modulated by the sintering atmosphere.[31,32] That is, if TiO_2 nanoparticles are used as catalysts for the growth of SWNT, the SWNT/TiO_2 interface can be altered by varying the synthesis conditions, which leaves plenty of space for the structure-controlled growth of SWNT arrays since we know the interfacial interaction between nanotube and catalyst is vital to the structures and properties of SWNTs. In addition, TiO_2 nanoparticles have much higher melting point compared with traditional metal catalysts. Therefore, they are generally assumed remaining in a solid state during the CVD process which is favorable for the structure control of SWNTs.[23,33] Besides, solid TiO_2 nanoparticles reduce the active catalysts aggregation and obviously increase the efficiency of catalysts,[34] more likely to realize the dense SWNT arrays. Meanwhile, the problem of residual metallic catalysts was resolved for the further application of SWNTs. These indicate that TiO_2 nanoparticles might be effective catalysts for the controlled growth of SWNT arrays.

Here, through the CVD process, we intend to utilize the oxygen vacancies in TiO_2 nanoparticles to affect the interaction between the nanoparticles and their grown SWNTs for inhibiting the formation of m-SWNTs. Thus, a feasible approach to realize the selective growth of horizontally aligned dense s-SWNTs using TiO_2 nanoparticles as catalysts was developed. Figure 1a schematically illustrated the procedure of the approach. First, the precursors of TiO_2 nanoparticles were dispersed onto ST-cut quartz substrates and then underwent thermal treatment to form catalytic TiO_2 nanoparticles (the details described in Methods). Figure S1a showed the typical atomic force microscope (AFM) image of the catalyst TiO_2 nanoparticle line (widths 5–10 μm) after annealing. The size distribution of most TiO_2 particles was within 0.8–1.9 nm with an average diameter of 1.46 nm (Figure S1b). X-ray photoelectron spectroscopy (XPS) was applied to investigate the states of catalyst nanoparticles. In the Ti $2p_{3/2}$ region, only

DOI: 10.1021/nl5037325
Nano Lett. 2015, 15, 403–409

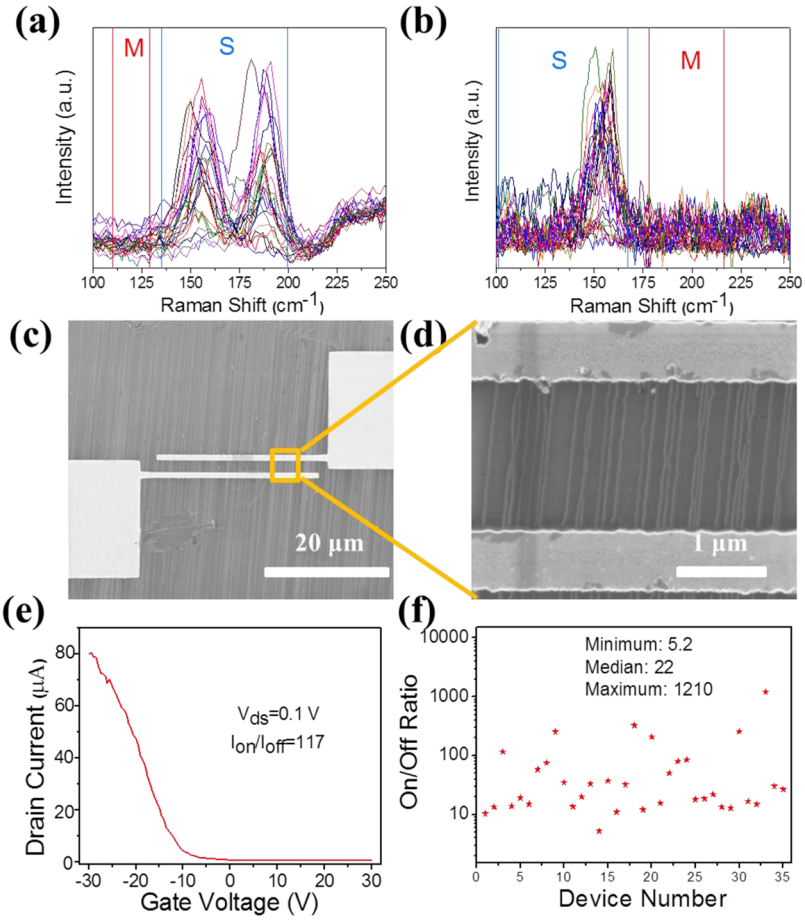

Figure 2. (a–b) Radial breathing mode (RBM) peaks of the Raman spectra for the as-grown SWNT samples transferred onto the SiO_2/Si substrates with 514 and 633 nm excitation. Peaks within the full line rectangles marked with S corresponded to the semiconducting SWNTs. The full line rectangles marked with M denoted the frequency range where RBM peaks of metallic SWNTs were expected; (c–d) SEM images of FET devices fabricated on the as-grown SWNT arrays transferred onto SiO_2/Si substrate; (e) a typical transfer characteristic curve of s-SWNTs device with V_{ds} = 100 mV; (f) the statistical result of I_{on}/I_{off} ratios for each device.

binding energy 458.5 eV (Ti^{4+}) corresponding to TiO_2 was detected[27,31] (Figure S2a, 2b). To avoid possible metal contamination in the CVD system, a new quartz tube and plastic tweezers were specially used for every growth process. The growth experiments were performed in a 1 in. tube furnace at 830 °C by introducing a flow of 200 standard cubic centimeters per minute (sccm) hydrogen and 200 sccm argon (through an ethanol bubbler). After 30 min of growth, the sample was cooled to room temperature and inspected with XPS. There were no metallic titanium peaks or titanium carbide peaks observed in the Ti 2p regions (Figure S2b). However, in the Ti $2p_{3/2}$ region, two peaks associated with two phases of titanium dioxide appeared (Figure S2d), one phase with the Ti^{4+} $2p_{3/2}$ peak at 458.5 eV and the other with the Ti^{3+} $2p_{3/2}$ peak at 457.2 eV. The lower binding energy signal is attributed to an oxygen-deficient phase of titanium dioxide, while the higher binding energy signal is attributed to stoichiometric TiO_2. Thus, the introduction of hydrogen and carbon source at elevated temperature did not reduce the TiO_2 to metal Ti but instead pulls off some oxygen atoms to yield oxygen vacancies. The oxygen-deficient TiO_2 nanoparticles were found the successful growth of the uniform, dense, and perfectly aligned SWNT arrays with larger areas from scanning electron microscope (SEM) observations (Figure 1b,c). Higher magnification SEM image (Figure 1c) and AFM image (Figure 1d) showed the average density of the arrays around 10 SWNTs per micron, local density over 15 SWNTs per micron. Figure 1e was the corresponding diameter analysis of the SWNTs which revealed a narrow distribution of 1.2 ± 0.3 nm. The mean diameter of grown SWNTs was smaller than the average size of oxygen-deficient TiO_2 nanoparticles, which was in accordance with relationships between the metallic nanoparticles and their grown SWNTs.[35]

To further confirm that TiO_2 nanoparticles are responsible for the nanotube growth under the CVD conditions, we performed certain control experiments. In the first typical control experiment, two clean SiO_2/Si wafers with a layer of 300 nm SiO_2 were used as the substrates. TiO_2 catalysts were dispersed onto one substrate by the spin-coating method (2000 r/s, 1 min) without any patterning step. No catalysts were put on the surface of the other substrate. These two substrates underwent the same growth conditions (the details of CVD process described in Methods). From SEM observations (Figure S3a,b), dense SWNT networks were obtained on the substrate loaded with TiO_2 catalysts (Figure S3a), while no SWNT was founded on the other substrate without any catalyst (Figure S3b). The general CVD growth was conducted under atmospheric pressure in 1 in. quartz tube which was heated by a tube furnace (TF 55035C-1 Lindberg/Blue M). We performed another control experiment in a different CVD system. The

DOI: 10.1021/nl5037325
Nano Lett. 2015, 15, 403–409

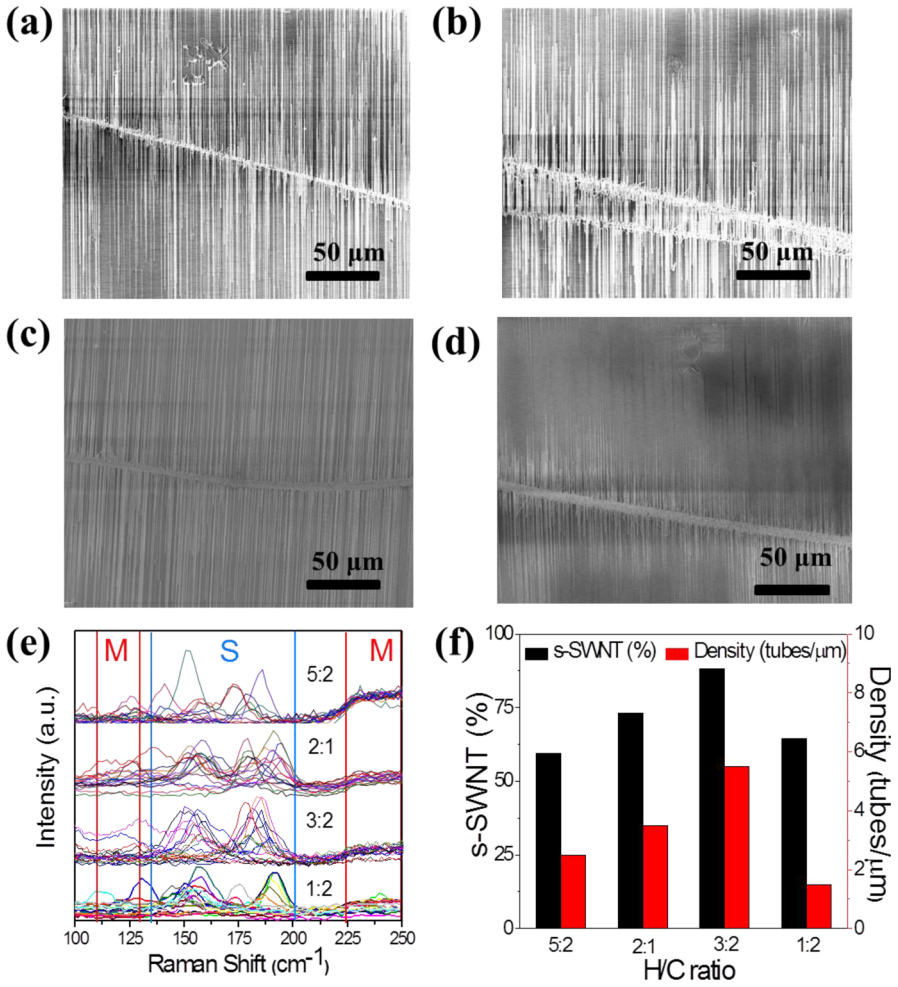

Figure 3. SEM images (a–d) and RBM peaks (e) of the SWNT arrays using TiO_2 nanoparticles as catalysts under the H/C ratios were 5:2, 2:1, 3:2, and 1:2, the Raman spectra with 514 excitation; (f) the statistics of density and s-SWNT percent in the as-grown SWNT arrays under different H/C ratios.

oven used was OTF-1200X tube furnace (Hefei Kejing Materials Technology Co.) with 2 in. quartz tube. The preparations of ST-cut quartz substrates and TiO_2 catalysts were the same in the general CVD growth. After the CVD process (the details described in Methods), close-packed SWNT arrays were obtained as shown in Figure S3c. These control experiments directly excluded the possibility that metal contaminant induced by the patterning method or by thermal evaporation of metal containing compounds were responsible for the nanotube growth. Combining with the results of other experiments mentioned above, such as the AFM image of the TiO_2 catalysts formed on the catalyst line (most TiO_2 particle size within 0.8–1.9 nm which suitable for the growth of SWNTs) and XPS spectra of TiO_2 catalysts before and after SWNTs growth (no metallic titanium peaks or other metal contaminant peaks observed), we can ensure that the growth of nanotubes is from TiO_2 nanoparticles.

Multiple excitation lasers (wavelengths of 514, 633, and 785 nm) combined with electrical measurements were used to characterize electronic properties of the as-grown SWNT arrays. Figure 2a and b were typical radial breathing mode (RBM) peaks of the Raman spectra for the SWNT samples with 514 and 633 nm excitation. It was quickly apparent that s-SWNT peaks were the overwhelming majority, with m-SWNTs peaks barely present. Raman measurements of multibatch samples demonstrated an amazing result that the percentage of s-SWNTs in the arrays was up to 97% by counting the numbers of RBMs based on multiwavelength laser (Figure S4). In addition, the barely noticeable D bands at high-frequency region reflect the aligned SWNTs arrays have high qualities (Figure S5). To further verify the high percentage of s-SWNTs in these samples, we carried out the electrical measurements in the field effect transistors (FET) forms by transferring SWNT arrays onto SiO_2/Si substrates. The fabrication and test processes of the FET devices were described in detail in Methods. Figure 2c and d were the low and high magnification SEM images of a representative FET structure with a channel length of 1.5 μm and width of 30 μm containing dozens of SWNTs. The I_{ds}–V_g curve was shown in Figure 2e with an on/off current ratio of ~117, which revealed typical semiconducting behavior of the channel materials. 35 similar FET devices were fabricated, and the corresponding on/off ratio distribution was plotted in Figure 2f. The median value of the on/off ratio is 22, with the minimum value as 5.2 and maximum value as 1210. Assuming all carbon nanotubes have similar on-state resistivity, the percentage of semiconducting nanotubes can be estimated to be above 95% according the median on/off ratio of 22.[7,15] The results of electrical measurements were consistent with the results obtained by Raman measurements. The analysis presented above clearly indicated we successfully

DOI: 10.1021/nl5037325
Nano Lett. 2015, 15, 403–409

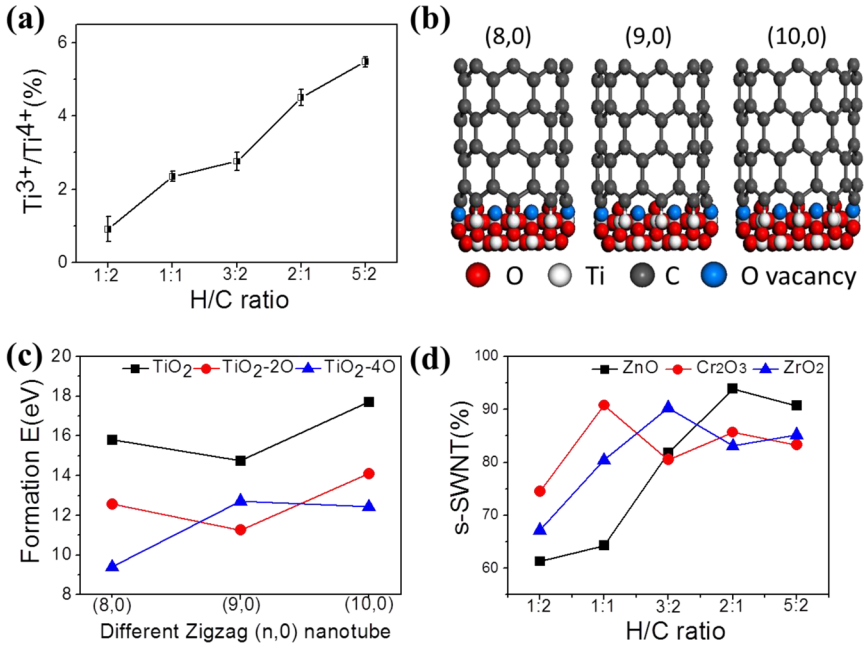

Figure 4. (a) Relationship between H/C ratio and peak areas Ti^{3+}/Ti^{4+} by XPS; (b) the structure models of (8,0), (9,0), and (10,0) SWNTs on the TiO_2 catalyst model with four oxygen vacancies; (c) the theoretically calculated formation energies between SWNTs and the TiO_2 surface with different concentrations of oxygen vacancies; (d) a statistical analysis about the ratio of semiconducting SWNTs in the SWNT arrays using a series of oxide nanoparticles as catalysts under different H/C ratios.

achieved semiconducting enriched and densely packed SWNT arrays using the oxygen-deficient TiO_2 nanoparticles as catalysts.

Verifying our hypothesis that oxygen vacancies in TiO_2 nanoparticles played a key role for the formation of close packed s-SWNT arrays is vital. According to the reported literatures,[31,32,36] the concentration of oxygen vacancies in TiO_2 nanoparticles has a significant impact on their surface properties and the formation energy with adsorbate. In addition, as mentioned above, the concentration can be modulated by the sintering atmosphere. So we varied the flow rate of hydrogen and argon (through an ethanol bubbler) which was defined as H/C ratio here, to obtain different concentration of oxygen vacancies samples at the same growth temperature and total flow. The ratio of peak areas in XPS spectrum corresponding to Ti^{3+} $2p_{3/2}$ and Ti^{4+} $2p_{3/2}$ directly reflected the amount of oxygen vacancies in TiO_2 nanoparticles.[32] Figure 4a was the relationship diagram of the H/C ratio and peak areas Ti^{3+}/Ti^{4+}. With the increasing of the H/C ratio from 1/2 to 5/2, the ratio of peak areas increased from 0.91% to 5.48%, suggesting more oxygen vacancies were produced. Figure 3a–d were the typical SEM images of the as-grown SWNT arrays under diverse H/C ratios. The average density declined obviously, from 10 tubes/μm dropping to 5 tubes/μm, or even lower when the H/C ratio deviated from the previous value 1:1 (Figure 3f). Additionally, a significant amount of metallic peaks were founded in Figure 3e when varying the H/C ratio. The percentages of s-SWNTs in these samples examined by multiwavelength laser Raman decreased significantly compared to the H/C ratio 1:1; typical results were less than 90% (Figure 3f). Combining with the above experimental results, we suppose that the optimized H/C ratio during the CVD growth results in a suitable concentration of oxygen vacancies in TiO_2 nanoparticles. Under such condition, the formation energy between s-SWNT and catalyst is lower than that of metallic SWNT (m-SWNT), which is in favor of the formation of s-SWNTs. Meanwhile, the suitable concentration of oxygen vacancies in TiO_2 nanoparticles is more conducive to maintain the activity of the catalysts during the growth of SWNTs, which accordingly realizes the dense s-SWNT arrays.

To better understand the importance of oxygen vacancy in nanosized TiO_2 at the molecular level for the selective growth of s-SWNT, we calculated the formation energy between SWNTs and the TiO_2 catalyst by using density functional theory (DFT) and plane wave basis.[37,38] In the calculation, (8,0), (9,0), and (10,0) SWNTs, among them the (9,0) tube is conducting, were selected. The TiO_2 catalyst was modeled by a (6 × 3) supercell (17.754 Å × 19.491 Å) of the (110) surface. Two layers of TiO_2 slab model were used in the calculation. The supercell dimension perpendicular to the TiO_2 surface was 30 Å in order to avoid the interactions between neighboring images. SWNTs were put on the same locations of the TiO_2 catalyst surface, and the oxygen atoms of the surface were removed to form oxygen vacancies (see the schematic diagram in Figure S6). Figure 4b depicted the models of (8,0), (9,0), and (10,0) SWNTs on the TiO_2 catalyst with four oxygen vacancies.

The calculated formation energies were presented in Table S1 and shown in Figure 4c. For the s-SWNTs in the case of no oxygen vacancy, the formation energy of metallic (9,0) SWNT with TiO_2 catalyst was 14.744 eV, which was smaller than the those of other two s-SWNTs′, 15.791 and 17.702 eV for (8,0) and (10,0) SWNTs, respectively. This clearly indicates the preference of growing metallic (9,0) SWNT. When there were two oxygen vacancies, the formation energies decreased, but the tendency of growing more metallic ones remained. While, when there were four oxygen vacancies on the TiO_2 catalyst surface, the formation energy of the s-SWNTs (8,0) and (10, 0), 9.406 and 12.435 eV, respectively, were smaller than that of the metallic SWNT (9,0), 12.716 eV. This means in favor of growing semiconducting SWNTs which is different from the

DOI: 10.1021/nl5037325
Nano Lett. 2015, 15, 403–409

situation of without or with less oxygen vacancy. In the other words, the oxygen vacancy in the TiO_2 catalyst must affect the preferential growth of s-SWNT greatly.

However, due to the complicated interplay of many factors in SWNT growth, the theoretical calculation model might be oversimplified in relative to real condition of SWNT growth, in which the shape of the catalyst particle might be not flat and there might be other forms of carbon elements appeared near the interface of the SWNT−catalyst particle. Meanwhile, we do see some agreement between the theoretical calculations and the experimental results—the formation energy between s-SWNT and the TiO_2 catalyst becomes smaller than that between m-SWNT and the catalyst (or s-SWNT becomes more stable than m-SWNT) under a certain concentration of oxygen vacancy (Figure 4c).

To rule out the possibility that the oxygen in ethanol may play an important role for the selective growth of semiconducting SWNTs, CH_4 was used as the carbon feeding gas. Through varying the flow rate of hydrogen and methane during the CVD process, close-packed aligned SWNTs were obtained as shown in Figure S7a. The percentage of s-SWNTs in the arrays was above 93% according to the statistics by multi-wavelength laser (Figure S7b). These results demonstrated the selectivity indeed originated from oxygen-deficient TiO_2 nanoparticles used. Understanding the role of oxygen vacancy in the preferential growth process of dense s-SWNT may provide insights into the interactions between nanoparticles and SWNTs at elevated temperatures. Furthermore, this method can also be extended to other series of semiconductor oxide nanoparticles (i.e., ZnO, ZrO_2, and Cr_2O_3) for the growth of dense s-SWNT arrays just optimizes the H/C ratio. The percentage of s-SWNTs varied with the H/C ratio as shown in Figure 4d. Representative SEM images of s-SWNT arrays from different oxide nanoparticles were observed in Figure S8.

In summary, we develop a feasible and effective method to realize selective growth of semiconducting and close-packed SWNT arrays using oxygen-deficient TiO_2 nanoparticles as catalysts. Average density of ∼10 tubes/μm, horizontally aligned semiconducting SWNTs on quartz wafers were successfully obtained. Both of Raman spectra and electrical measurement results indicated that above 95% of the SWNTs in the arrays were semiconducting tubes. Detailed experimental and theoretical studies reveal that oxygen vacancies in TiO_2 nanoparticles played a key role for the selective growth of semiconducting SWNTs. A suitable concentration of oxygen vacancies in TiO_2 nanoparticles can form by optimizing the flow rate of hydrogen and carbon source during the process of SWNT growth. Under such conditions, TiO_2 nanoparticles have smaller formation energy between s-SWNT than metallic SWNT (m-SWNT), which is in favor of growing s-SWNT. Additionally, this strategy can be applied to other semiconductor oxide nanoparticles (i.e., ZnO, ZrO_2, and Cr_2O_3) for the selective growth of dense s-SWNT arrays. These results offer more choices for the structure-control growth of SWNTs which are beneficial to both fundamental research and future applications in nanoelectronics.

■ ASSOCIATED CONTENT

Supporting Information

Description of experimental details, calculated results listed in the table, and supplementary figures. This material is available free of charge via the Internet at http://pubs.acs.org.

■ AUTHOR INFORMATION

Corresponding Authors

*E-mail: qwli2007@sinano.ac.cn.
*E-mail: jinzhang@pku.edu.cn.

Author Contributions

J.Z., Q.L., and L.K. designed the experiment. L.K., Y.H., J.W., S.Z., and Q.Z. performed the experiments and analyzed the results. L.L. and F.D. performed the theoretical calculation. J.Z., Q.L. L.K., Y.H., J.W., S.Z., Q.Z., L.L., and F.D. contributed to the writing and discussion of the manuscript.

Notes

The authors declare no competing financial interest.

■ ACKNOWLEDGMENTS

We are grateful to Dr. Liming Xie (National Center for Nanoscience and Nanotechnology, China) and Rong Jian (Peking University, China) for their helpful discussions about scanning electronic microscopy. This work was supported by NSFC (21233001, 21129001, 51272006, 51432002, and 51121091) and MOST (2011CB932601).

■ REFERENCES

(1) Che, Y. C.; Chen, H. T.; Gui, H.; Liu, J.; Liu, B. L.; Zhou, C. W. *Semicond. Sci. Technol.* **2014**, *29*, 073001.
(2) Shulaker, M. M.; Hills, G.; Patil, N.; Wei, H.; Chen, H. Y.; Wong, H. S. P.; Mitra, S. *Nature* **2013**, *501*, 526−530.
(3) Shulaker, M. M.; Van Rethy, J.; Wu, T. F.; Suriyasena Liyanage, L.; Wei, H.; Li, Z. Y.; Pop, E.; Gielen, G.; Wong, H. S. P.; Mitra, S. *ACS Nano* **2014**, *8*, 3434−3443.
(4) Franklin, A. D. *Nature* **2013**, *498*, 443−444.
(5) Cao, Q.; Han, S. J.; Tulevski, G. S.; Zhu, Y.; Lu, D. D.; Haensch, W. *Nat. Nanotechnol.* **2013**, *8*, 180−186.
(6) Wang, Y. L.; Pillai, S. K. R.; Chan-Park, M. B. *Small* **2013**, *9*, 2960−2969.
(7) Che, Y. C.; Wang, C.; Liu, J.; Liu, B. L.; Lin, X.; Parker, J.; Beasley, C.; Wong, H. S. P.; Zhou, C. W. *ACS Nano* **2012**, *6*, 7454−7462.
(8) Ding, L.; Tselev, A.; Wang, J. Y.; Yuan, D. N.; Chu, H. B.; McNicholas, T. P.; Li, Y.; Liu, J. *Nano Lett.* **2009**, *9*, 800−805.
(9) Chen, Y. B.; Zhang, J. *Acc. Chem. Res.* **2014**, *47*, 2273−2281.
(10) Chen, Y. B.; Zhang, Y. Y.; Hu, Y.; Kang, L. X.; Zhang, S. C.; Xie, H. H.; Liu, D.; Zhao, Q. C.; Li, Q. W.; Zhang, J. *Adv. Mater.* **2014**, *26*, 5898−922.
(11) Ding, L.; Yuan, D. N.; Liu, J. *J. Am. Chem. Soc.* **2008**, *130*, 5428−5429.
(12) Zhou, W. W.; Ding, L.; Yang, S.; Liu, J. *ACS Nano* **2011**, *5*, 3849−3857.
(13) Hong, S. W.; Banks, T.; Rogers, J. A. *Adv. Mater.* **2010**, *22*, 1826−1830.
(14) Wu, B.; Geng, D. C.; Guo, Y. L.; Huang, L. P.; Chen, J. Y.; Xue, Y. Z.; Yu, G.; Liu, Y. Q.; Kajiura, H.; Li, Y. M. *Nano Res.* **2011**, *4*, 931−937.
(15) Zhou, W. W.; Zhan, S. T.; Ding, L.; Liu, J. *J. Am. Chem. Soc.* **2012**, *134*, 14019−14026.
(16) Yu, B.; Liu, C.; Hou, P. X.; Tian, Y.; Li, S. S.; Liu, B. L.; Li, F.; Kauppinen, E. I.; Cheng, H. M. *J. Am. Chem. Soc.* **2011**, *133*, 5232−5235.
(17) Hong, G.; Zhang, B.; Peng, B. H.; Zhang, J.; Choi, W. M.; Choi, J. Y.; Kim, J. M.; Liu, Z. F. *J. Am. Chem. Soc.* **2009**, *131*, 14642−14643.
(18) Zhang, Y. Y.; Zhang, Y.; Xian, X. J.; Zhang, J.; Liu, Z. F. *J. Phys. Chem. C* **2008**, *112*, 3849−3856.
(19) Qin, X. J.; Peng, F.; Yang, F.; He, X. H.; Huang, H. X.; Luo, D.; Yang, J.; Wang, S.; Liu, H. C.; Peng, L. M.; Li, Y. *Nano Lett.* **2014**, *14*, 512−517.
(20) Hong, G.; Chen, Y. B.; Li, P.; Zhang, J. *Carbon* **2012**, *50*, 2067−2082.

DOI: 10.1021/nl5037325
Nano Lett. 2015, 15, 403−409

(21) Wang, H.; Goh, K.; Xue, R.; Yu, D. S.; Jiang, W. C.; Lau, R.; Chen, Y. *Chem. Commun.* **2013**, *49*, 2031−2033.
(22) He, M. S.; Liu, B. L.; Chernov, A. I.; Obraztsova, E. D.; Kauppi, I.; Jiang, H.; Anoshkin, I.; Cavalca, F.; Hansen, T. W.; Wagner, J. B.; Nasibulin, A. G.; Kauppinen, E. I.; Linnekoski, J.; Niemelä, M.; Lehtonen, J. *Chem. Mater.* **2012**, *24*, 1796−1801.
(23) Yang, F.; Wang, X.; Zhang, D. Q.; Yang, J.; Luo, D.; Xu, Z. W.; Wei, J. K.; Wang, J. Q.; Xu, Z.; Peng, F.; Li, X. M.; Li, R. M.; Li, Y. L.; Li, M. H.; Bai, X. D.; Ding, F.; Li, Y. *Nature* **2014**, *510*, 522−524.
(24) Sanchez-Valencia, J. R.; Dienel, T.; Groning, O.; Shorubalko, I.; Mueller, A.; Jansen, M.; Amsharov, K.; Ruffieux, P.; Fasel, R. *Nature* **2014**, *512*, 61−64.
(25) Yao, Y. G.; Feng, C. Q.; Zhang, J.; Liu, Z. F. *Nano Lett.* **2009**, *9*, 1673−1677.
(26) Liu, B. L.; Ren, W. C.; Gao, L. B.; Li, S. S.; Pei, S. F.; Liu, C.; Jiang, C. B.; Cheng, H. M. *J. Am. Chem. Soc.* **2009**, *131*, 2082−2083.
(27) Cai, Q. R.; Hu, Y. L.; Liu, Y. Y.; Huang, S. M. *Appl. Surf. Sci.* **2012**, *258*, 8019−8025.
(28) Huang, S. M.; Cai, Q. R.; Chen, J. Y.; Qian, Y.; Zhang, L. J. *J. Am. Chem. Soc.* **2009**, *131*, 2094−2095.
(29) Chen, H. H.; Nanayakkara, C. E.; Grassian, V. H. *Chem. Rev.* **2012**, *112*, 5919−5948.
(30) Jourdain, V.; Bichara, C. *Carbon* **2013**, *58*, 2−39.
(31) Chen, X. B.; Liu, L.; Yu, P. Y.; Mao, S. S. *Science* **2011**, *331*, 746−750.
(32) Ganduglia-Pirovano, M. V.; Hofmann, A.; Sauer, J. *Surf. Sci. Rep.* **2007**, *62*, 219−270.
(33) Bachilo, S. M.; Balzano, L.; Herrera, J. E.; Pompeo, F.; Resasco, D. E.; Weisman, R. B. *J. Am. Chem. Soc.* **2003**, *125*, 11186−11187.
(34) Zhang, L. L.; Liu, C.; Liu, B. L.; Yu, W. J.; Hou, P. X.; Cheng, H. M. *Carbon* **2013**, *55*, 253−259.
(35) Cheung, C. L.; Kurtz, A.; Park, H.; Lieber, C. M. *J. Phys. Chem. B* **2002**, *106*, 2429−2433.
(36) Zuo, F.; Wang, L.; Wu, T.; Zhang, Z. Y.; Borchardt, D.; Feng, P. Y. *J. Am. Chem. Soc.* **2010**, *132*, 11856−11857.
(37) Kresse, G.; Furthmuller, J. *Phys. Rev. B* **1996**, *54*, 11169.
(38) Kresse, G.; Furthmuller, J. *Comput. Mater. Sci.* **1996**, *6*, 15−50.

DOI: 10.1021/nl5037325
Nano Lett. 2015, 15, 403−409